This is a repository copy of *The effect of heating rate on discontinuous grain boundary alpha formation in a metastable beta titanium alloy*.

White Rose Research Online URL for this paper:
https://eprints.whiterose.ac.uk/162047/

Version: Published Version

Article:
Gao, J. and Rainforth, W.M. orcid.org/0000-0003-3898-0318 (2020) The effect of heating rate on discontinuous grain boundary alpha formation in a metastable beta titanium alloy. Metallurgical and Materials Transactions A, 51 (8). pp. 3766-3771. ISSN 1073-5623

https://doi.org/10.1007/s11661-020-05856-4

Reuse
This article is distributed under the terms of the Creative Commons Attribution (CC BY) licence. This licence allows you to distribute, remix, tweak, and build upon the work, even commercially, as long as you credit the authors for the original work. More information and the full terms of the licence here: https://creativecommons.org/licenses/

Takedown
If you consider content in White Rose Research Online to be in breach of UK law, please notify us by emailing eprints@whiterose.ac.uk including the URL of the record and the reason for the withdrawal request.

eprints@whiterose.ac.uk
https://eprints.whiterose.ac.uk/

Communication

The Effect of Heating Rate on Discontinuous Grain Boundary Alpha Formation in a Metastable Beta Titanium Alloy

JUNHENG GAO and W. MARK RAINFORTH

Continuous grain boundary α (α_{GB}) is often observed in age-hardened metastable β titanium alloys and plays a detrimental role in ductility. In this work, we show that the heating rate to the aging temperature is crucial in determining the extent of α_{GB}. The extent of α_{GB} is determined by the extent of formation of isothermal ω at grain boundaries. This new finding is significant for suppressing continuous α_{GB} formation in aging hardened β titanium alloys.

https://doi.org/10.1007/s11661-020-05856-4
© The Author(s) 2020

Metastable β titanium alloys have been extensively studied in recent years due to their high strength-to-density ratio, good hardenability, and excellent fatigue behavior, which are promising properties for light-weighting of vehicles with the advent of rapid global climate change and alarming levels of atmospheric CO_2 concentrations.[1–4] In precipitation-hardened metastable β titanium alloys, the volume fraction and morphology of α precipitates control the strength level and hence the strength-to-density ratio.[1,2,5–7] In order to achieve superfine intragranular α precipitates, extensive studies have focused on the mechanisms and pathways for the intragranular α precipitation.[1,8–11] It has been suggested that ω phase and/or pseudospinodal decomposition of β phase is an important part of the nucleation of α precipitates.[8–10,12–15] Recently, Zheng *et al*. reported that ω phase provides an extra driving force for the copious nucleation of intragranular α precipitates.[9,12,13] They suggested that low heating rate leads to the formation isothermal ω precipitates, resulting in compositional and structural non-uniformities in the β matrix. These then act as preferential sites for heterogeneous nucleation of α precipitates, leading to a highly refined dispersion of α precipitates in grain interior.[9,12,13,16–18]

Although the effect of ω phase on the formation of intragranular α precipitates has been extensively studied, its effect on the α_{GB} formation has not been reported. The allotriomorphic distribution of α phase along prior β grain boundaries with the formation Widmanstatten α plates is typical microstructure of near-α and α + β titanium alloys in the solid solution and aged condition.[13,19,20] However, in precipitation-strengthened metastable β titanium alloys, continuous grain boundary α (α_{GB}) is frequently observed after aging.[1,16,21–25] The formation of continuous α_{GB} at grain boundaries will reduce the hardness of grain boundaries, which results in large mechanical contrast between grain boundaries the precipitation-hardened matrix, thereby leading to fracture from the prior β grain boundaries.[21,26–28] Therefore, the suppression of continuous α_{GB} may aid ductility and fracture toughness of precipitation-strengthened metastable β titanium alloys.

The current work was inspired by the influence of ω phase on the precipitation of intragranular α precipitates.[9,12,13,17,18,29] We systemically studied the role of ω phase in α_{GB}formation using low heating rates up to the aging temperature. After annealing at 820 °C for 10 minutes, three different heating rates to 350 °C, 400 °C, and 480 °C (4 °C/min, 2 °C/min, and 0.5 °C/min) for aging were used and the aged alloys were systematically studied by scanning electron microscopy (SEM), transmission electron microscopy (TEM), and scanning transmission electron microscopy (STEM). We found that ω phase plays an important role for the suppression of continuous α_{GB}.

The Ti-1.5Al-8Mo-3Cr-2.5Fe (wt pct) alloy was arc melted from pure elements in a high-purity argon atmosphere. The ingot was homogenized at 1170 °C for 5 hours under flowing argon and water quenched. It was then hot rolled at 1000 °C from 23 to 13 mm thickness and water quenched. The hot-rolled plate was cold rolled from 13 to 6.2 mm in 5-6 pct strain increments, followed by annealing at 1000 °C for 5 minutes and water quenched. The plate was finally cold rolled from 6.2 to 1.2 mm in 5-6 pct strain increments. The thin plate was annealed at 820 °C for 10 minutes under flowing argon, followed by water quenching. After annealing, the plate was cut into nine parts. Six of them were heated to 350 °C and 400 °C at three different heating rates (4 °C/min, 2 °C/min, and 0.5 °C/min), which are denominated 350-4, 350-2, 350-0.5, 400-4, 400-2, and 400-0.5, and water quenched immediately. Two of them were heated to 480 °C at two different heating rates (4 °C/min and 0.5 °C/min) and held for 2 hours, followed by water quenching. The heat treatment procedure is outlined in Figure 1. Samples for SEM were mechanically ground and polished down to

JUNHENG GAO and W. MARK RAINFORTH are with the Department of Materials Science and Engineering, The University of Sheffield, Sheffield S1 3JD. Contact emails: junheng.gao@sheffield.ac.uk; m.rainforth@sheffield.ac.uk
Manuscript submitted March 9, 2020.

Published online: 08 June 2020

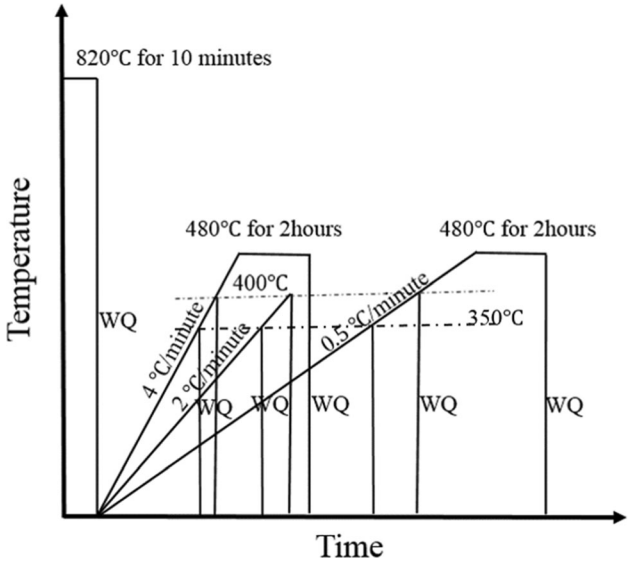

Fig. 1—Schematic diagram of heat treatment procedure used in this study.

1 μm diamond suspension, followed by polishing using a Gatan precision etching coating system (PECS™) II system at 3 kV, 5 deg for 20 minutes for backscatter electron (BSE) imaging using a field emission gun scanning electron microscope (FEI Inspect F50 FEG SEM) operated at 10 kV. Samples for TEM were mechanically ground to ~ 100 μm in thickness and punched to 3-mm-diameter discs and then these 3-mm-diameter discs were twin-jet electropolished with a solution of 5 pct perchloric acid, 35 pct 2-butoxyethanol, and 60 pct methanol at − 35 °C. An FEI Tecnai T20 TEM operated at 200 kV was used to characterize the annealed and aged samples. A high-angle annular dark-field scanning transmission electron microscopy (HAADF-STEM) (JEOL F200) coupled with energy-dispersive spectroscopy was used to investigate possible formation of continuous α_{GB} in the alloy after aging at 480 °C for 2 hours with a heating rate of 0.5 °C/min.

Figure 2 presents the microstructure of Ti-1.5Al-8Mo-3Cr-2.5Fe after annealing at 820 °C for 10 minutes. As shown in Figure 2(a), the annealed alloy shows typical equiaxed grains with a size in the range of 5-120 μm. Figure 2(b) shows the dark-field TEM micrograph of the annealed alloy, recorded using the reflection marked by the red arrow in the selected area electron diffraction (SAED) pattern shown in the inset of Figure 2(b). The indexed $[110]_{\beta}$ zone axis diffraction pattern identified the presence of athermal hexagonal ω phase in the β matrix. Figure 2(b) shows the distribution of ω phase, with a size in the range of 0.5-3 nm.

As the formation of isothermal ω phase depends on the heating rate to the aging temperature,[5,9,12,16,30] we used three heating rates, namely 4 °C/min, 2 °C/min, and 0 °C/min to 350 °C and 400 °C, to study whether ω phase formed or not at the grain boundary. Figure 3 shows the dark-field TEM images of 350-4, 350-2, and

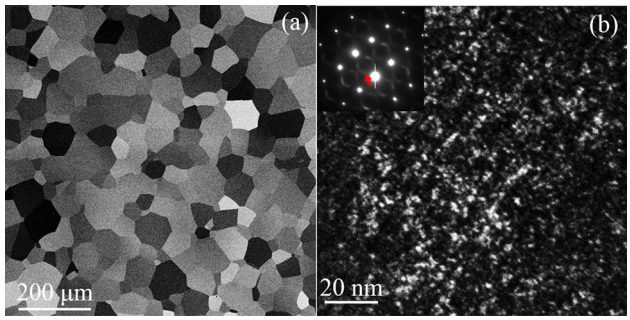

Fig. 2—(*a*) BSE SEM image of Ti-1.5Al-8Mo-3Cr-2.5Fe annealed at 820 °C for 10 min and quenched to room temperature. (*b*) Dark-field TEM image recorded using the red arrow marked spot in the inset showing the distribution of ω precipitates of the Ti-1.5Al-8Mo-3Cr-2.5Fe alloy heat-treated as in (a); inset is the corresponding SAED pattern of $[110]_{\beta}$ zone axis.

350-0.5 alloys and insets are their corresponding $[110]_{\beta}$ zone axis SAED patterns. As shown in Figure 3(a), extensive formation of isothermal ω phase in grain interior was observed after heating to 350 °C at a heating rate of 4 °C/min. The size of intragranular ω in 350-4 alloy was measured in the range 1-9 nm. For 350-2 alloy (Figure 3(b)), ω phase in the grain interior was in the range 1-8 nm and a higher number density was observed than for 350-4 alloy. The ω phase for 350-0.5 alloy (Figure 3(c)) was 1-8 nm in size with the highest number density of the three alloys. No ω-depleted zone was observed at grain boundaries for the above three alloys.

Figure 4 presents the dark-field TEM images of 400-4, 400-2, and 400-0.5 alloys and insets are their corresponding $[110]_{\beta}$ zone axis SAED patterns. As shown in Figure 4(a), extensive formation of isothermal ω phase in grain interior was observed after heating to 400 °C at a heating rate of 4 °C/min. However, a ω-depletion zone with a width of ~ 20 nm was observed at the grain boundary (marked by yellow dashed line in Figure 4(a)). The size of intragranular ω in 400-4 alloy was measured in the range 2-13 nm. For 400-2 alloy (Figure 4(b)), ω phase in the grain interior (size range 3-23 nm) had coarsened more due to the lower heating rate than for 400-4 alloy. Moreover, fine ω phase with a size in the range of 2-3 nm was observed at the grain boundary, as marked by the yellow dashed lines in Figure 4(b). When the heating rate for aging decreased to 0.5 °C/min (Figure 4(c)), the size of intragranular ω phase was 5-30 nm and no ω-depletion zone was observed at grain boundaries.

Figure 5 shows BSE SEM micrographs of Ti-1.5Al-8Mo-3Cr-2.5Fe aged at 480 °C for 2 hours at a heating rate of 4 °C/min (Figure 5(a)) and 0.5 °C/min (Figures 5(b) and (c)). For a heating rate of 4 °C/min (Figure 5(a)), continuous $\alpha_{GB}$was observed. Moreover, Widmanstatten α plates were also observed at the grain boundary. For the alloy with a heating rate of 0.5 °C/min, a discontinuous distribution of α_{GB} was observed. The discontinuous distribution of α_{GB} was highlighted by blue arrows in the zoom-in image of Figure 5(c).

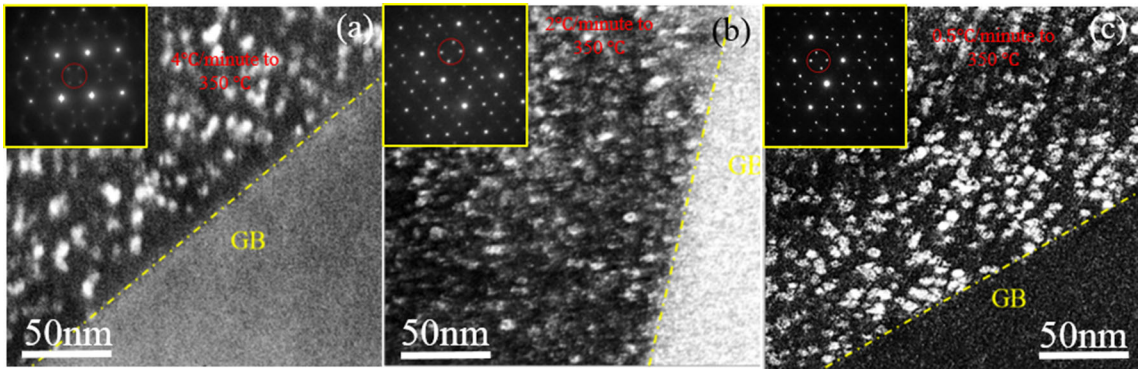

Fig. 3—Dark-field TEM images of water-quenched Ti-1.5Al-8Mo-3Cr-2.5Fe alloy after annealing at 820 °C for 10 min, followed by different heating rates to 350 °C and water-quenched immediately. (*a*) 4 °C/min; (*b*) 2 °C/min; (*c*) 0 °C/min. Dark-field TEM images were recorded using the red circle marked spots as shown in the insets. Insets are their corresponding SAED patterns of $[110]_{\beta}$ zone axis. The dashed yellow lines are drawn to highlight the grain boundaries (Color figure online).

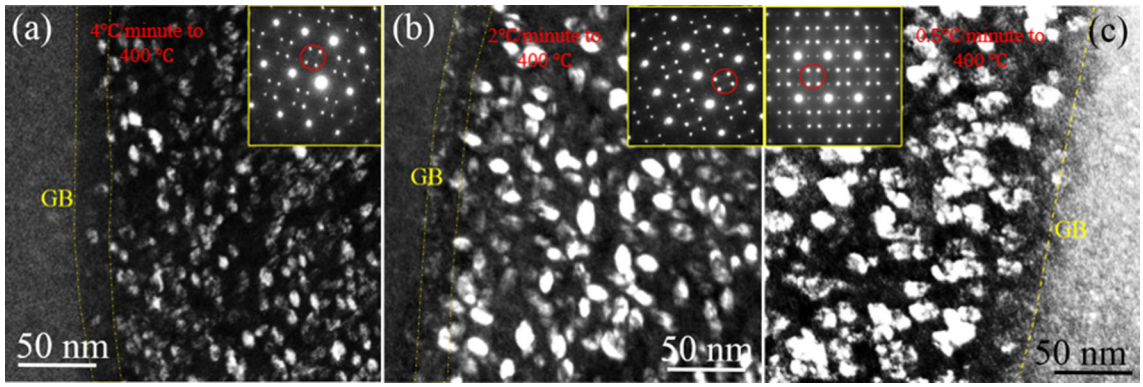

Fig. 4—Dark-field TEM images of water-quenched Ti-1.5Al-8Mo-3Cr-2.5Fe alloy after annealing at 820 °C for 10 min, followed by different heating rates to 400 °C and water-quenched immediately. (*a*) 4 °C/min; (*b*) 2 °C/min; (*c*) 0 °C/min. Dark-field TEM images were recorded using the red circle marked spots as shown in the insets. Insets are their corresponding SAED patterns of $[110]_{\beta}$ zone axis. The dashed yellow lines are drawn to highlight the grain boundaries (Color figure online).

Moreover, in comparison with the size of intragranular α precipitates in Figure 5(a), the intragranular α precipitates in Figure 5(b) are much finer, which is consistent with reports that lower heating rates to the aging temperature leads to finer intragranular α precipitates.[9,16]

The grain boundaries of aged Ti-1.5Al-8Mo-3Cr-2.5Fe alloys were studied by TEM and STEM (Figure 6). The formation of continuous α_{GB} and Widmanstatten α plates was further confirmed for Ti-1.5Al-8Mo-3Cr-2.5Fe with a heating rate of 4 °C/min, as observed in the bright-field TEM images in Figure 6(a). For Ti-1.5Al-8Mo-3Cr-2.5Fe with a heating rate of 0.5 °C/min, discontinuous α_{GB} was also confirmed by TEM, as shown in the bright-field image of Figure 6(b) (highlighted by blue arrows). In order to confirm that the bright grain boundary phase in Figure 6(b) is α phase and the ubiquity of discontinuous α_{GB} formation at grain boundaries for Ti-1.5Al-8Mo-3Cr-2.5Fe with a heating rate of 0.5 °C/min, STEM and EDS line scan were conducted. HAADF-STEM image in Figure 6(c) clearly shows the discontinuous distribution of α_{GB} (highlighted by blue arrows), which is consistent with Figure 5(b) and (c), and corresponding EDS line scan (Figure 6(d)) shows that α phase was poor in β stabilizers Mo, Cr, and Fe, while rich in Al. The inset of Figure 6(c) is the zoom-in image of the red rectangle marked region in Figure 6(c), which highlights the discontinuous distribution of α_{GB}. Four more random selected grain boundaries are shown in Electronic Supplementary Figure S1, which also confirms the distribution of discontinuous α_{GB} and some grain boundaries without obvious α_{GB} distribution were also observed.

The suppression of continuous α_{GB} is crucial to achieve both high strength and high ductility, especially in precipitation-strengthened metastable β titanium alloys.[21–24] However, similar to $\alpha+\beta$ titanium alloys,[22,31] the preferential nucleation and growth of α phase at β grain boundaries during aging makes it difficult to avoid.[22] The most efficient route to alleviate the α_{GB} formation is wrought processing,[32] but this

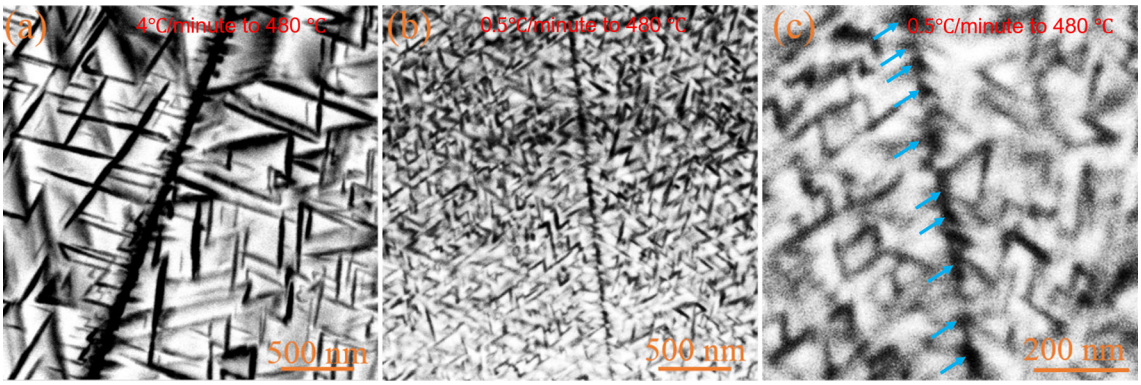

Fig. 5—BSE SEM micrographs of Ti-1.5Al-8Mo-3Cr-2.5Fe annealed at 820 °C for 10 min, followed by water quenching to room temperature and heating to 480 °C at a heating rate of 4 °C/min (*a*) and 0.5 °C/min (*b* and *c*) and then held for 2 h. (*c*) The zoom-in image of (b) highlighting the discontinuous distribution of α_{GB} (highlighted by blue arrows in (c)) (Color figure online).

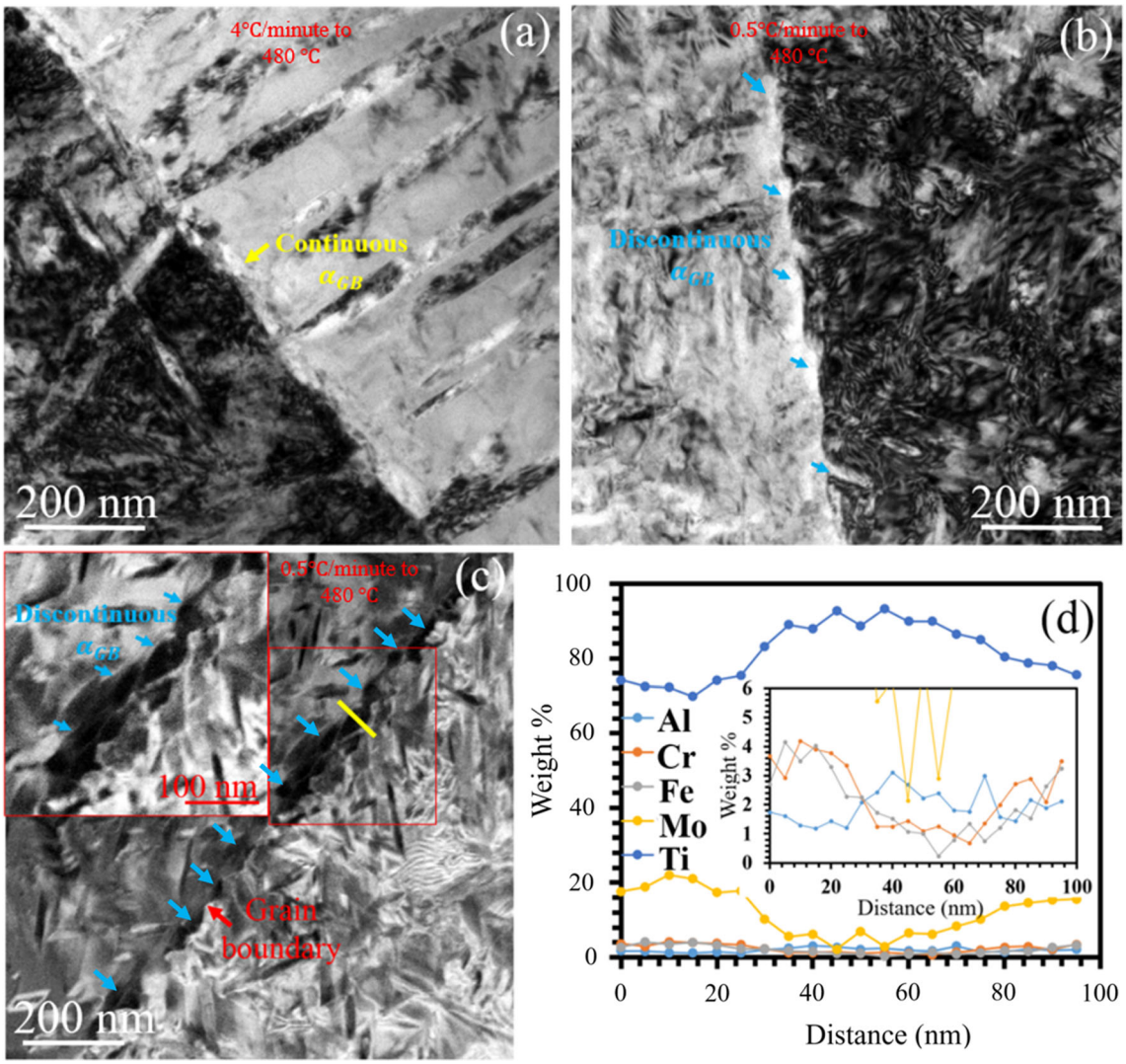

Fig. 6—TEM and STEM study of aged Ti-1.5Al-8Mo-3Cr-2.5Fe. The alloys were annealed at 820 °C for 10 min, followed by aging at 480 °C for 2 h at a heating rate of 4 °C/min (*a*) and 0.5 °C/min (*b*) and (*c*). (a) and (b) Bright-field TEM micrographs. (c) HAADF-STEM image (inset: zoom-in image of red rectangle marked region in (c)). (*d*) STEM-EDS line scan (marked by yellow line in (c)). The discontinuous distribution of α_{GB} in the alloy with 0.5 °C/min is highlighted by blue arrows in (b) and (c) (Color figure online).

route is not applicable to the promising near-net-shape processing methods, such as additive manufacturing.[22–25] This is because wrought process will break the shape of part after additive processing. In this work, we found that the formation of continuous α_{GB} can be alleviated by using low heating rates to the aging temperature, which is applicable to the additive manufacturing parts. It is worth noting that all the heating rates used in this work were lower than the reported lowest heating rate (5 °C/min) previously reported for the refinement of intragranular α precipitates.[9,16] This finding is significant because it suggests that even for a low heating rate, such as 2 °C/min, there is a ω-depletion zone at the grain boundary and that further decreasing the heating rate can avoid the formation of a ω-depleted zone at grain boundaries. As suggested in References 9, 13, and 17, the isothermal ω phase in grain interiors could play a direct or indirect role for the copious nucleation of intragranular α precipitates. Therefore, the presence of isothermal ω phase at grain boundaries is supposed to aid the heterogenous nucleation of α phase at the grain boundaries,[17] leading to discontinuous distribution of α phase at grain boundaries.

As observed in Figure 3, ω phase was observed at the grain boundaries for the 350-4, 350-2, 350-0.5 alloys, while for the 400-4 and 400-2 alloys, ω-depletion zones were observed. This indicates that grain boundary ω phase transformed to β phase during the temperature increase from 350 °C to 400 °C in the 400-4 and 400-2 alloys. This finding is consistent with Zheng's work that an increase of aging temperature can destabilize both isothermal ω and α phase formed at 350 °C, leading to both ω to β and α to β transformation.[9,12,13] It is well established that the growth of isothermal ω phase requires the partitioning of alloy elements, which is clearly time and temperature dependent.[16,30,33] For the 4 °C/min and 2 °C/min heating rate-treated alloys, the size and volume fraction of ω phase at the grain boundary was smaller than that of 0.5 °C/min heating rate-treated alloy (Figures 3 and 4). This was because the more rapid heating gave less time for ω nucleation and growth and alloying element partitioning, resulting in smaller ω and less significantly partitioning of β stabilizers in comparison with that of the 350-0.5 alloy. In comparison with grain interiors, the diffusion rate of alloying elements at the grain boundary was faster.[34] With increasing annealing temperature from 350 °C to 400 °C, the faster diffusion rate at grain boundaries facilitated the homogenous distribution of β stabilizers at grain boundaries, which further destabilized ω phase at grain boundaries, thereby resulting in the formation of ω-depletion zone at the grain boundaries in the 5 °C/min and 2 °C/min heating rate-treated alloys. However, for the 0.5 °C/min heating rate-treated alloy, the volume fraction and size of the ω phase was significantly larger than that of 4 °C/min and 2 °C/min heating rate-treated alloys (Figures 3 and 4). This suggests that ω phase was better stabilized due to the lower heating rate (longer heating/aging time) which resulted in greater alloying element partitioning, so longer annealing time was required for the homogeneous distribution of alloying elements in the 5 °C/min heating rate-treated alloy. As a result, ω phase was retained at grain boundaries at 400 °C for 400-0.5 alloys. With an increase of temperature from 400 °C to 480 °C, the ω precipitates at grain boundaries play a direct or indirect role in the heterogenous nucleation of α precipitates at grain boundaries, leading to the formation of discontinuous α_{GB}.

In summary, our results suggest that in order to alleviate the formation of continuous α_{GB} in metastable β titanium alloys, low heating rates (0.5 °C/min) need to be applied. This new finding is significant for the production of high-strength and high-ductility precipitate-strengthened metastable β titanium alloys, especially for near-net-shape processing methods, such as additive manufacturing, where wrought processing is not applicable.

This work was supported by the EPSRC project "Designing Alloys for Resource Efficiency (DARE)," EP/L025213/1 and the Henry Royce Institute for supplying transmission electron microscope (JEOL F200).

ELECTRONIC SUPPLEMENTARY MATERIAL

The online version of this article (https://doi.org/10.1007/s11661-020-05856-4) contains supplementary material, which is available to authorized users.

OPEN ACCESS

This article is licensed under a Creative Commons Attribution 4.0 International License, which permits use, sharing, adaptation, distribution and reproduction in any medium or format, as long as you give appropriate credit to the original author(s) and the source, provide a link to the Creative Commons licence, and indicate if changes were made. The images or other third party material in this article are included in the article's Creative Commons licence, unless indicated otherwise in a credit line to the material. If material is not included in the article's Creative Commons licence and your intended use is not permitted by statutory regulation or exceeds the permitted use, you will need to obtain permission directly from the copyright holder. To view a copy of this licence, visit http://creativecommons.org/licenses/by/4.0/.

REFERENCES

1. A. Devaraj, V.V. Joshi, A. Srivastava, S. Manandhar, V. Moxson, V.A. Duz, and C. Lavender: *Nat. Commun.*, 2016, vol. 7, p. 11176.
2. S.A. Mantri, D. Choudhuri, T. Alam, G.B. Viswanathan, J.M. Sosa, H.L. Fraser, and R. Banerjee: *Scripta Mater.*, 2018, vol. 154, pp. 139–44.

3. J.L. RuifengDong, H. Kou, J. Fan, and B. Tang: *J. Mater. Sci. Technol.*, 2019, vol. 35, pp. 48–54.
4. J. Gao, A.J. Knowles, D. Guan, and W.M. Rainforth: *Scripta Mater.*, 2019, vol. 162, pp. 77–81.
5. O.M. Ivasishin, P.E. Markovsky, Y.V. Matviychuk, S.L. Semiatin, C.H. Ward, and S. Fox: *J. Alloys Compd.*, 2008, vol. 457, pp. 296–309.
6. N.G. Jones, R.J. Dashwood, M. Jackson, and D. Dye: *Scripta Mater.*, 2009, vol. 60, pp. 571–73.
7. R. Dong, J. Li, H. Kou, J. Fan, and B. Tang: *J. Mater. Sci. Technol.*, 2019, vol. 35, pp. 48–54.
8. S. Nag, Y. Zheng, R.E.A. Williams, A. Devaraj, A. Boyne, Y. Wang, P.C. Collins, G.B. Viswanathan, J.S. Tiley, B.C. Muddle, R. Banerjee, and H.L. Fraser: *Acta Mater.*, 2012, vol. 60, pp. 6247–56.
9. Y. Zheng, R.E.A. Williams, J.M. Sosa, T. Alam, Y. Wang, R. Banerjee, and H.L. Fraser: *Acta Mater.*, 2016, vol. 103, pp. 165–73.
10. T. Li, D. Kent, G. Sha, H. Liu, S.G. Fries, A.V. Ceguerra, M.S. Dargusch, and J.M. Cairney: *Scripta Mater.*, 2018, vol. 155, pp. 149–54.
11. Q. Xue, Y.J. Ma, J.F. Lei, R. Yang, and C. Wang: *J. Mater. Sci. Technol.*, 2018, vol. 34, pp. 2325–30.
12. Y. Zheng, R.E.A. Williams, J.M. Sosa, Y. Wang, R. Banerjee, and H.L. Fraser: *Scripta Mater.*, 2016, vol. 111, pp. 81–84.
13. Y. Zheng, R.E.A. Williams, D. Wang, R. Shi, S. Nag, P. Kami, J.M. Sosa, R. Banerjee, Y. Wang, and H.L. Fraer: *Acta Mater.*, 2016, vol. 103, pp. 850–58.
14. Y. Zheng, D. Choudhuri, T. Alam, R.E.A. Williams, R. Banerjee, and H.L. Fraser: *Scripta Mater.*, 2016, vol. 123, pp. 81–85.
15. A. Devaraj, S. Nag, R. Srinivasan, R.E.A. Williams, S. Banerjee, R. Banerjee, and H.L. Fraser: *Acta Mater.*, 2012, vol. 60, pp. 596–609.
16. P. Barriobero-Vila, G. Requena, S. Schwarz, F. Warchomicka, and T. Buslaps: *Acta Mater.*, 2015, vol. 95, pp. 90–101.
17. F. Prima, P. Vermaut, G. Texier, D. Ansel, and T. Gloriant: *Scripta Mater.*, 2006, vol. 54, pp. 645–48.
18. T. Li, D. Kent, G. Sha, M.S. Dargusch, and J.M. Cairney: *Scripta Mater.*, 2015, vol. 104, pp. 75–78.
19. T. Ahmed and H.J. Rack: *Mater. Sci. Eng. A*, 1998, vol. 243, pp. 206–11.
20. R. Shi, V. Dixit, H.L. Fraser, and Y. Wang: *Acta Mater.*, 2014, vol. 75, pp. 156–66.
21. J.W. Foltz, B. Welk, P.C. Collins, H.L. Fraser, and J.C. Williams: *Metall. Mater. Trans. A*, 2011, vol. 42A, pp. 645–50.
22. C. Liu, Y. Lu, X. Tian, and D. Liu: *Mater. Sci. Eng. A*, 2016, vol. 661, pp. 145–51.
23. C.M. Liu, H.M. Wang, X.J. Tian, and D. Liu: *Mater. Sci. Eng. A*, 2014, vol. 604, pp. 176–82.
24. G. Lütjering, J. Albrecht, C. Sauer, and T. Krull: *Mater. Sci. Eng. A*, 2007, vols. 468–470, pp. 201–09.
25. C.M. Liu, H.M. Wang, X.J. Tian, and H.B. Tang: *Mater. Sci. Eng. A*, 2014, vol. 590, pp. 30–36.
26. S. Osovski, A. Srivastava, J.C. Williams, and A. Needleman: *Acta Mater.*, 2015, vol. 82, pp. 167–78.
27. C. Huang, Y. Zhao, S. Xin, C. Tan, W. Zhou, Q. Li, and W. Zeng: *Inter. J. Fatig.*, 2017, vol. 94, pp. 30–40.
28. Z. Yan, K. Wang, Y. Zhou, X. Zhu, R. Xin, and Q. Liu: *Scripta Mater.*, 2018, vol. 156, pp. 110–14.
29. Y. Ohmori, T. Ogo, K. Nakai, and S. Kobayashi: *Mater. Sci. Eng. A*, 2001, vol. 312, pp. 182–88.
30. J. Coakley, B.-S. Seong, D. Dye, and M. Ohnuma: *Phil. Mag. Lett.*, 2017, vol. 97, pp. 83–91.
31. J. Gao, J. Nutter, X. Liu, D. Guan, Y. Huang, D. Dye, and W.M. Rainforth: *Sci. Rep.*, 2018, vol. 8, pp. 7512–11.
32. G. Lütjering and J.C. Williams: *Titanium*, Springer, Berlin, 2007.
33. S.A. Mantri, D. Choudhuri, T. Alam, V. Ageh, F. Sun, F. Prima, and R. Banerjee: *Scripta Mater.*, 2017, vol. 130, pp. 69–73.
34. P.P. Chattopadhyay, S.K. Pabi, and I. Manna: *Mater. Chem. Phys.*, 2001, vol. 68, pp. 80–84.

Publisher's Note Springer Nature remains neutral with regard to jurisdictional claims in published maps and institutional affiliations.